Eur. J. Mineral.
PrePub DOI: 10.1127/ejm/2019/0031-2871

PrePub Article

Distribution of trace elements in willemite from the Belgium non-sulphide deposits

Flavien CHOULET[1,*], James RICHARD[1], Marie-Christine BOIRON[2], Augustin DEKONINCK[3] and Johan YANS[3]

[1]Chrono-Environnement UMR 6249, CNRS-Université de Bourgogne Franche-Comté, 25030 Besançon, France
*Corresponding author, e-mail: flavien.choulet@univ-fcomte.fr
[2]GeoRessources UMR 7359, CNRS-Université de Lorraine, 54506 Nancy, France
[3]Département de Géologie, Institute of Life, Earth and Environment, Université de Namur, 5000 Namur, Belgium

Abstract: Samples of willemite (Zn_2SiO_4) mineralization from the historical non-sulphide Zn–Pb deposits of La Calamine (eastern Belgium) have been recovered from collections of the Geological Survey of Belgium. Textural and chemical analyses are used to evaluate the critical element distribution (Ge, In, Ga) and deportment. willemite occurs as a variety of types that continuously formed between the protore stage (sulphides) and the late supergene stage (carbonates and hydrated phases). Different types of willemite may be distinguished on the basis of their shape and zoning characteristics, supporting a polyphase non-sulphide mineralization after the protore stage. This is also marked by a significant change of major-element compositions in the late generation of willemite. Laser-ablation inductively coupled plasma mass-spectrometry (LA-ICP-MS) measurements of minor and trace elements also reveal a strong variability between the different willemite types, although no straightforward relation with the shape of willemite crystals or their zoning is demonstrated. Among the trace elements, we note anomalous high contents of P, Cd, As, Pb, Ag and Sb, the three latter ones being related to tiny galena inclusions. While Ga and In contents are very low (less than 4 ppm) or below detection limits, respectively, significant Ge contents up to 250 ppm were measured. Such contents are consistent with values reported from willemite mineralization throughout the world. The concentrations measured in willemite are similar to those in sphalerite (averaging 250 ppm), supporting a role as precursor for sphalerite. However, the supergene origin of willemite in Belgian deposits is controversial and the influence of low-temperature hydrothermal fluids for willemite precipitation cannot be ruled out. This also questions the origin of Ge further incorporated in zinc silicates.

Key-words: willemite; germanium; non-sulphide zinc deposits; critical elements; supergene.

1. Introduction

The supergene zone of sulphide-rich ore deposits has long been a focus for the mining industry, as fractionation processes due to weathering can lead to significant metal enrichment relative to the primary ore. Oxidation of sulphide minerals results in the formation of a range of oxides, secondary sulphides, carbonates and even silicates. Since processing of such minerals has less impact on the environment (*e.g.*, reduced acid mine drainage, limited volumes of tailings and flotation wastes), they were reconsidered for mining exploration during the last decades. Supergene zones are also known as targets for precious metals, as secondary gold and silver enrichment is common, especially for Volcanic Massive Sulphide (VMS) deposits (*e.g.*, Yesares *et al.*, 2014; Reich & Vasconcelos, 2015). Investigation of the supergene zone of Zn–Pb deposits during the past 20 years has contributed to reconsider historical deposits and exploration of new ones throughout the world (see review of Boni & Mondillo, 2015). These deposits represent a sub-class of non-sulphide zinc deposits (Hitzman *et al.*, 2003), which are characterized by the predominance of zinc oxides, carbonates and silicates (including clays and hydrated phases) over sulphide minerals. Numerous studies undertaken worldwide have led to a good understanding of formation mechanisms and robust metallogenic models, implying the replacement of primary sulphides by secondary minerals under specific weathering conditions and favourable tectonic settings or host rocks (*e.g.*, Boni *et al.*, 2003; Borg, 2009; Choulet *et al.*, 2014; Verhaert *et al.*, 2017).

In the protore, sphalerite is known to accommodate a number of cations due to various substitutions (*e.g.*, Cook *et al.*, 2009, 2015; Ye *et al.*, 2011; Belissont *et al.*, 2014), including some of the critical metals (Ge, Ga, In). Mechanisms for incorporation can be related to crystallographic processes, as sphalerite may display faces, sectors or bands that present significant differences in minor-element abundance (Belissont *et al.*, 2014, 2016). For example, Ge content can reach up to 1000s ppm, representing one of the major sources for recovering this minor metal (Höll *et al.*, 2007; Cook *et al.*, 2009). The behaviour of germanium

0935-1221/19/0031-2871 $ 6.75

and other minor elements during weathering of primary sulphides is poorly understood or even documented. While some minor metals are hosted in carbonates (*e.g.*, cadmium; Schwartz, 2000), other mineral phases such as hydroxides and silicates are known to incorporate significant amounts of critical elements, and especially germanium (Bernstein, 1986; Lombaard *et al.*, 1986; Saini-Eidukat *et al.*, 2009; Choulet *et al.*, 2017; Mondillo *et al.*, 2018a, b). As direct replacement textures are frequently reported, the initial content of sulphide minerals is a determining factor for the final concentration of trace elements in the secondary minerals. Although the amount of Ge may locally reach several thousands ppm (*e.g.*, Saini-Eidukat *et al.*, 2009), this element can be heterogeneously distributed within host mineral phases (*e.g.*, in willemite; Choulet *et al.*, 2017). As mentioned above for sphalerite, this could indicate that the concentration of trace elements in secondary phases also depends on crystallographic parameters of the host mineral. External supply of minor elements by hydrothermal fluids and competition between secondary host minerals are also crucial features to determine the potential of the supergene zone. This has major implication for exploration and recovery of Ge during mineral and metallurgical processing (Drzazga *et al.*, 2018).

Based on the example of the Belgian non-sulphide deposits, we attempt to evaluate the exploration potential of secondary non-sulphide minerals hosting strategic metals, taking into account their complex mineralogical evolution. Belgian non-sulphide deposits around the La Calamine locality are historical deposits, which have produced zinc from carbonate and silicate ores (Dejonghe *et al.*, 1993), until to the development of flotation and the generalization of sulphide ore processing at the beginning of the 20th century. La Calamine is also the type locality for willemite (Cesàro, 1887) and, despite the total closure of mines and their flooding, numerous samples are currently available in museum collections. While previous studies focused on mineralogical inventorying or determining of conditions for Belgium non-sulphide ore formation (Coppola *et al.*, 2008), the distribution of minor metals remains under-investigated, despite significant Ge and Ga concentrations in the primary sulphides (Goffin *et al.*, 2015). This study presents detailed observation and analyses of sulphide and non-sulphide zinc ores and aims at diagnosing their potential for strategic metals such as Ge, as future exploration of these deposits is still a matter of debate in Belgium (Goossens, 2014).

2. Geological setting

2.1. Regional geology

Belgium has a long mining history mainly due to the occurrence of numerous Zn–Pb deposits within the Palaeozoic bedrock of the Dinant, Namur and Verviers synclinoria (Dejonghe, 1998). The geology of Belgium is closely associated to the evolution of the Variscan Belt and especially of the Rheno-Hercynian Zone (Franke, 2000). Successive tectonic (and minor metamorphic) events led to the formation of a composite Palaeozoic basement that was further covered by Permian to Quaternary sediments (Fig. 1). The Palaeozoic basement includes Cambrian to Ordovician sedimentary rocks, further deformed and metamorphosed by Caledonian (*sensu lato*) events (Michot, 1980; Fielitz & Mansy, 1999). A first regional unconformity ("Ardennian") is the result of a tilting of the pre-Silurian basement, while a second regional unconformity ("Brabantian") represents the effect of tectonic inversion during the Early Devonian (Sintubin *et al.*, 2009). Afterwards, a first cover made of Devonian to Carboniferous sedimentary rocks was deposited in a new platform associated with the development of the Rheic Ocean (Oncken *et al.*, 1999). A new episode of inversion tectonics, related to the Variscan orogeny, started at the end of the Viséan and sedimentation was accompanied by the formation of regional inverse faults, such as the Midi Fault zone (Meilliez & Mansy, 1990). These thrusts accommodated the overthrusting of the southern Ardenne allochthon over the northern Brabant parautochthon. Consequently, regional-scale folded units, like the Dinant and Namur synclinoria developed and represent, with the Brabant parautochthon, the present-day structural zones of Belgium (Belanger *et al.*, 2012). Further discontinuous Permian to recent sedimentary cover is recorded throughout the northern part of the country. Successive uplift episodes during the Mesozoic and the Cenozoic have progressively contributed to a partial erosion of this cover, and the subaerial exposure of the Paleozoic rocks (Vercautere & van den Haute, 1993; Quesnel, 2003; Thiry *et al.*, 2006; Demoulin *et al.*, 2018). To the northeast of Belgium (Fig. 1), Lower Cretaceous sandstone, siltstone and clays of the Aachen, Vaals and Gulpen formations cover the Early Palaeozoic rocks of the Verviers Synclinorium, the eastern prolongation of the "Dinant Synclinorium" (Graulich *et al.*, 1984). Early Palaeozoic rocks include sandstones, shales, and carbonates; they are crosscut by two sets of faults: (1) NE-SW trending reverse faults related to the Variscan episodes and (2) NNW-SSE faults linked with the inception of the Rhine Graben (Fig. 1).

2.2. Metallogeny of Zn–Pb deposits in Belgium

The Verviers Synclinorium was the most productive mining area of metals in Belgium, representing around 75% of the total national past production of Pb–Zn ore concentrates (Dejonghe *et al.*, 1993). Several types of primary sulphide ore deposits are distinguished: syn- to diagenetic veins and associated flats and palaeo-karst formations (Dejonghe, 1998). The distribution of ore deposits was largely controlled by the NNW-SSW faults (Fig. 1). The formation of sulphide orebodies resulted from hydrothermal events, which date back to the mid-Jurassic (Schneider *et al.*, 1999). They were related to high salinity fluids derived from the late evolution of the sedimentary basin during the Late Palaeozoic; fluids were further involved in diagenetic processes but remained trapped at depth until to Jurassic tectonic episodes, which allowed their remobilization (Heijlen *et al.*, 2001). The precipitation of sulphides resulted from mixing between metal-bearing fluids and fluids containing reduced sulfur (*e.g.*, Sangster, 1990), leading to consider

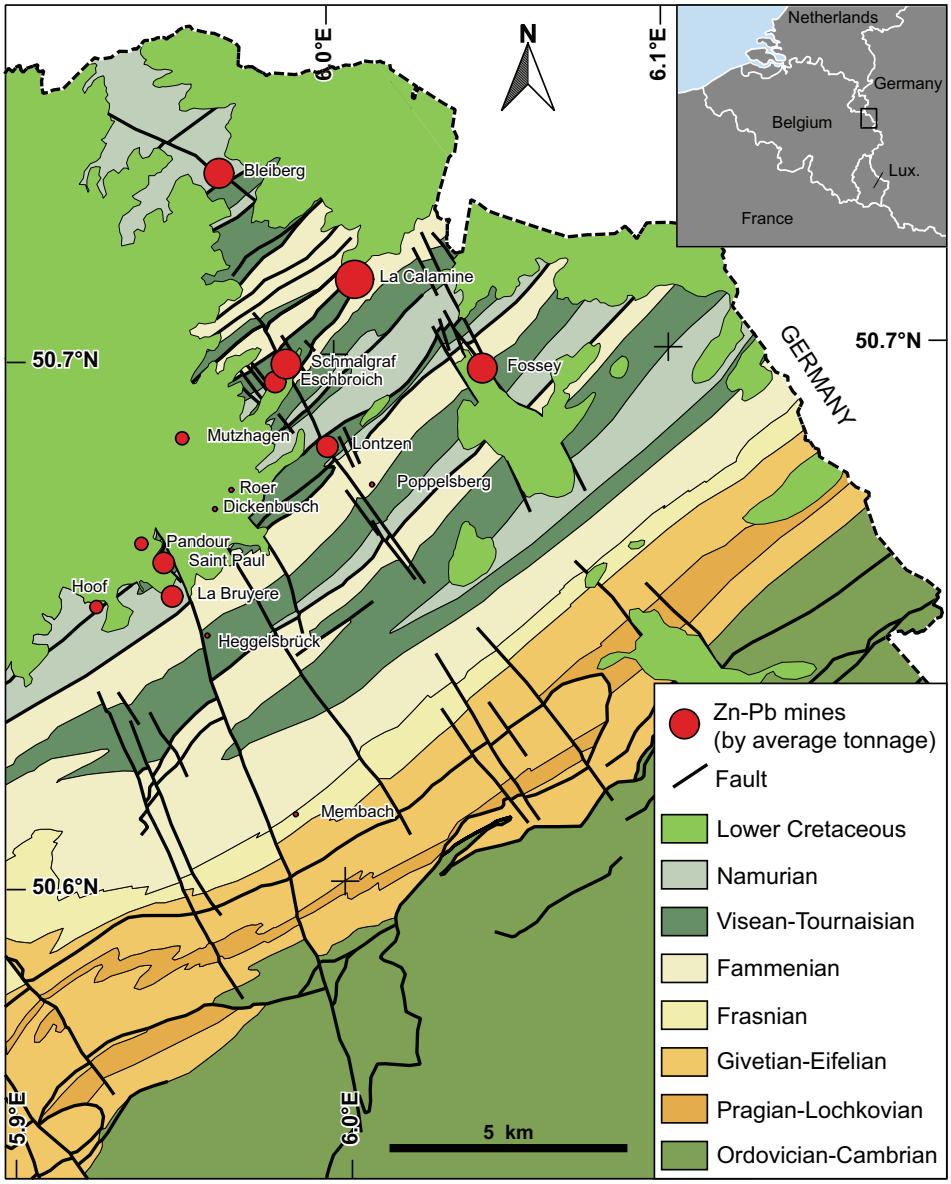

Fig. 1. Geological map of northeastern Belgium, with location of old Zn–Pb mines. Note the distribution of deposits along NNW-SSE trending faults. Size of red circle is proportional to metal tonnage (data from Dejonghe, 1998). Modified after Dejonghe & Jans (1983).

the Verviers ore deposits as Mississipi Valley type (MVT) deposits (Muchez *et al*., 1994, 2005). In addition, numerous non-sulphide ore deposits were formed by supergene weathering of the underlying primary sulphide deposits, with the exception of La Calamine (Dejonghe & Boni, 2005). The age of this oxidation event is probably Lower to Mid-Cretaceous (Coppola *et al*., 2008), consistent with various constraints on regional palaeo-weathering (*e.g*., Yans, 2003; Thiry *et al*., 2006; Demoulin *et al*., 2018) and the unconformity of Late Cretaceous rocks (Fig. 1). The La Calamine Mine, also referred to as Vieille Montagne or Moresnet, consists of a lenticular pocket with a sinkhole shape, hosted by Tournaisian dolomite and controlled by the position of a NE-SW thrust zone (Dejonghe, 1998). Sulphide minerals were found only in traces (Dejonghe & Jans, 1983) and were considered as of supergene origin, although Coppola *et al*. (2008) provided mineralogical evidence for a partial replacement of sphalerite by willemite. The mineralization consists of a mixture of non-sulphide minerals, including early willemite and late smithsonite, hemimorphite and zinc clays, forming the typical "Calamine" ores (Coppola *et al*., 2008). Based on stable isotopes and fluid inclusions, Boni *et al*. (2005) and Coppola *et al*. (2008) proposed that it is presently not possible to decide between supergene weathering and low-temperature hydrothermal process for the formation of willemite. The formation of the late non-sulphide minerals (carbonates) is unequivocally related to supergene processes, though (Coppola *et al*., 2008).

3. Material and methods

Since Belgian deposits are inaccessible, characterization of mineralogy was made on samples housed at the Geological Survey of Belgium of the Royal Belgian Institute of Natural Sciences (RBINS). Most of the samples come from the historical mine of La Calamine (Table 1). One sample (IG32105-259) was also collected from the Fossey Mine, located to the south of La Calamine mine; this deposit was characterized by veins and flat lenses, at the limit between the Famennian sandstone and shale and the Tournaisian dolomite (Dejonghe & Jans, 1983). Another sample (RN3874) originates from the small Heggelsbrück deposit in the southwestern part of the district, where ore mineralization consists of non-sulphide veins hosted by the Famennian formations (Fig. 1; Dejonghe & Jans, 1983).

Samples were cut to prepare polished thin sections. Optical investigation using a Leica DMRX petrographic microscope was supplemented by electronic microscopy using a Scanning Electron Microscope (SEM) at the FEMTO-ST Institute (Université de Bourgogne Franche-Comté, France). Backscattered Electron (BSE) imaging operating at 15 kV in low vacuum conditions was combined with semi-quantitative analysis using Energy-Dispersive Spectrometers (EDS). Cold Cathodoluminescence (CL) observations using OPEA instrumentation hosted at Chrono-Environnement (Université de Bourgogne Franche-Comté) were made with an acceleration voltage of 18.5 ± 1.5 keV and a current of 350 ± 150 mA to investigate zoning in willemite and establish relationships with other minerals.

Major-element composition of sphalerite, carbonates and willemite was obtained by Electron Probe Micro-Analysis (EPMA) at the University of Lausanne, Switzerland, using a JEOL 8200 Superprobe equipped with five Wavelength-Dispersive Spectrometers (WDS). Carbon-coated polished thin sections were analyzed with a beam of 15 kV and a current of 10 nA. The resolution was *ca.* 1 µm. Oxides, silicates, and pure metals were used as standards. Jeol house-procedures were used for data reduction and the limits of detection were between 100 ppm and 300 ppm for detected elements. In addition, X-ray intensity hyperspectral mapping was realized to disclose the specific textures caused by the chemical features of minerals, especially in sulphide minerals.

The Laser-ablation inductively coupled plasma mass-spectrometry (LA-ICP-MS) measurements of trace element contents within willemite and sphalerite were made on a quadripolar Agilent 7500c ICP-MS coupled with a 193-nm excimer (Geolas Q Plus System) laser hosted at GeoRessources, Nancy, France. Laser ablations were performed with a constant 5 Hz pulse rate at 90 mJ laser energy. The laser spot size was 44 µm in diameter. The total acquisition time (background and signal) was limited to 100 s for one spot. Zinc content previously measured by EPMA was used as an internal standard for willemite and sphalerite. For willemite, NIST 610 (Ge, 426 ± 10 ppm; Ga, 438 ± 11 ppm; In, 441 ± 32 ppm) and NIST 612 (Ge, 35 ± 3 ppm; Ga, 36 ± 2 ppm; In, 43 ± 4 ppm) were used as external standards (Pearce *et al.*, 1997). For sphalerite, we used Mass-1 (Ge 58 ± 3 ppm, Ga 64 ± 11 ppm and In concentrations of about 50 ppm) as external standard (Wilson *et al.*, 2002). As the amount of ablated material is different for each analysis, the detection limits (d.l.) are different for each analysis and each element. The d.l. was calculated following the procedure detailed in Longerich *et al.* (1996). A 3σ criterion was used to estimate the d.l., minimum values of which are lower than 1 ppm for the trace elements analysed with an ablation spot diameter of 44 µm. The following isotopes were monitored to evaluate the Ge content: ^{70}Ge, ^{72}Ge, ^{73}Ge, ^{74}Ge, and ^{76}Ge. ^{70}Ge, ^{72}Ge and ^{76}Ge were not considered due to interference with ^{70}Zn, ^{56}Fe^{16}O and Ar isotopes, respectively. Following Belissont *et al.* (2014), we chose to retain ^{74}Ge, the most abundant isotope (36.28%), for the quantification of Ge in willemite. Data reduction was carried out using Iolite 3.0 (Paton *et al.*, 2011).

4. Results

4.1. Optical and electron microscopy

Different morphologies of willemite can be observed in the non-sulphide samples. The most frequent one is marked by botryoidal sub-rounded aggregates that occur in druses. These 0.5 mm sized spherulites (Type *W*) consist of radially distributed elongated prisms (Fig. 2A) showing oscillatory zoning. In some cases, these oscillatory-zoned elongated prisms delimit a rim (W_R) around a hexagonal crystal remnant (W_C) in the core of the aggregate (Fig. 2B). This

Table 1. Sample location with brief description of macroscopic textures and mineralogy. Minerals are listed by their relative abundance.

Sample number	Locality	Description	Mineralogy
RN6483	La Calamine	Sulphide breccia with schalenblende	Sp, Gal, Py, Cal
RV2/837	La Calamine	Massive sulphide	Sp, Py, Gal
RN4019	La Calamine	Dissolution breccia with reddish willemite and clay filling	W, Sm, Cal, Sid, Clays, Qz, Zn–clays, Goe, Hem
RA5003	La Calamine	Massive microcrystalline willemite	W, Sm, Cal, Clays, Qz, Zn-clays, Zn–P
RA5232	La Calamine	Microglobular willemite aggregate with clay filling	W, Sph, Gal, Py, Clays, Qz Zn-clays, Dsc
RA6661	La Calamine	Microglobular willemite aggregate	W, Clays, Qz, Zn-clays, Goe, Hem, Zn–P
IG32105/259	Fossey	Carbonate-rich breccia	W, Qz, Sm, Sid
RN3874	Heggelsbrück	Porous microglobular willemite aggregate	W, Clays, Qz, Zn-clays, Goe, Hem, Zn–P

Cal, calcite; Dsc, descloizite; Gal, galena; Goet, goethite; Hem, hematite; Py, pyrite; Qz, quartz; Sid, siderite; Sm, smithsonite; W, willemite; Zn–P, undifferentiated zinc phosphates.

nucleus does not show regular internal zoning (Fig. 2C), but has probably slightly different crystallographic parameters, since interference colours are relatively distinct between the core (first order) and the outer rim (second order) (Fig. 2B). The core remnants can also be of larger size and sub-rectangular shape, with tiny and fibrous willemite in the rim that displays a comb-like texture (Fig. 2D). Locally, the core exhibits very complex internal structures, only revealed by CL imaging (Fig. 2E and F). Such cores formed in two steps: (1) development of idiomorphic and prismatic crystals with growth bands (W_{C1}), and (2) aggregation and cementation by slightly zoned willemite (W_{C2}). The formation of willemite may be accompanied by the formation of tiny crystals of Pb-bearing minerals, such as cerussite and galena (Gn) (Fig. 2G and H). Willemite also forms massive areas (W_2), which consist of tiny subeuhedral crystals intergrown with euhedral prismatic quartz crystals (Fig. 3A and B). Quartz (Qz) is characterized by a two stage crystallization with a sub-rounded deep-blue luminescent core, surrounded by a rim exposing bright yellowish colour in CL (Fig. 3A and C). Willemite (W_1), with distinctive luminescence and contrast/brightness characteristics in BSE imaging mode, is also observed in the massive facies (Fig. 3A–C). Sometimes, this type is well developed and we may observe internal zoning and growth banding (Fig. 3D), very similar to that of willemite rims (W_R) in other facies (Fig. 2).

The studied samples also include carbonates; they occur in veins that crosscut silicates (Fig. 3A, B and D, E) or as crystals coating willemite in druses. Veins include a mixture of smithsonite (Sm) with deep red luminescence and successive bands of zincian siderite (Zn–Sd) and Fe-rich smithsonite (Fe–Sm), with darker luminescence (Fig. 3A and D). Calcite (Cal) also occurs as late infilling within the secondary porosity formed by the dissolution of zinc and iron carbonates (Fig. 3D). The druses are also filled with detrital material including quartz and a mixture of K-rich clay minerals (Figs. 2B and 3F). Secondary minerals such as zinc clays, probably fraipontite (Fig. 3F), zinc phosphates (hopeite, scholzite or parascholzite) and zinc vanadates (descloizite) are also present as patches.

Sulphide samples are characterized by a "Schalenblende" texture formed by collomorphic concretions of sphalerite (Fig. 4A–D). The concretions are cemented by colourless sphalerite (Sp) intergrown with calcite (Fig. 4A) and expose rhythmic bands with various colours under the optical microscope (Fig. 4B and C). Within *schalenblende*, galena and pyrite (Py) crystals can also be observed (Fig. 4D and E). Sphalerite also occurs as relics within willemite. A rim of secondary galena coats the zinc sulphides, preserving the protore from further weathering (Fig. 4F).

4.2. Chemical composition of willemite, carbonates and sphalerite

A summary of willemite compositions is reported in Table 2. For all data, the sum of oxides is between 98% and 102% and the Si/Zn ratios are consistent with an ideal composition of willemite, and significantly differ from hemimorphite. Detailed analysis of individual spots is provided in Tables S1 and S2 in the Supplementary Material linked to this article and freely available at https://pubs.geoscienceworld.org/eurjmin. All willemite types distinguished in the previous section except W_2 have similar ZnO and SiO_2 contents, consistent with ideal stoichiometry (73.04 wt% for ZnO and 26.96 wt% for SiO_2). For W_2, we can observe excess ZnO, with a mean value reaching 74.12 wt%. Interpretation of such zinc excess is unclear and it could be related to the presence of crystal defects in the willemite structure or of nano-inclusions of Zn-bearing minerals. No difference can be seen for FeO and CaO. For the trace-element contents, the following observations can be made: the P and As contents are heterogeneous and may reach up to 4000 ppm. Except outliers, the Mn content is generally low (less than 75 ppm). The Pb content in willemite is mostly between 400 ppm and 1400 ppm, but concentration can be unusually high (W_{1b}) due to tiny galena inclusions (Fig. 2G and H). In this case, higher Cu, Ag and Sb contents are also measured. While the In content is below detection limits and the Ga content does not exceed 4 ppm, the average Ge contents range from 17 ppm to 68 ppm with a maximum value of 252 ppm. In zoned crystals, there is no clear difference in composition between core and rim, except for higher P content in the core. W_2 remarkably differs from other willemite types, as significantly lower Pb, As, Ge and Mn contents (means of 23, 5, 17 and 12 ppm respectively) and higher Cd contents (mean 47 ppm) are measured.

The chemical composition of carbonates was obtained by EPMA and is reported in Table 3. Detailed analysis of individual spots is provided in Table S3. In addition to pure calcite, studied samples include zinc and iron carbonates. Smithsonite contains major amounts of MgO (mean 2.0 wt%), but low amounts of CaO (mean 0.5 wt%) and FeO (mean 0.9 wt%). Pure smithsonite exhibits a red luminescence (Fig. 3A) and differs from dark luminescent smithsonite (Fig. 3D) in which the Fe content ranges from 9.0 wt% to 27.5 wt% (mean 15.5 wt%). The MgO and CaO contents are also significantly higher (means 3.5 and 1.1 wt%). Siderite is also present in samples (Fig. 3D) and carries high ZnO, MgO and CaO contents (means 6.9, 2.6 and 4.6 wt%, respectively).

The composition of sphalerite is provided in Table 4 and detailed analyses can be found in Tables S4 and S5. Sphalerite shows a variable Fe content, ranging from 0 wt % to 5 wt%. Sphalerite commonly contains significant minor elements including Cu, Ge, As, Cd, Sb and Pb. Dark bands in *schalenblende* (Fig. 5A) are marked by high Fe content, while light bands are iron-free (Fig. 5B). According to element maps, there is a clear negative correlation between Fe and Cd, at least in the inner parts of concretions (Fig. 5C). The Ge content ranges between 19 ppm and 1325 ppm within sphalerite, and averages 269 ppm and 246 ppm in the two samples. The In content is below detection limit and the Ga content is less than 3 ppm. This variability is due to heterogeneous element distribution and apparent correlation between the Fe and Ge contents (Fig. 5D and E). In other sulphides (galena and pyrite),

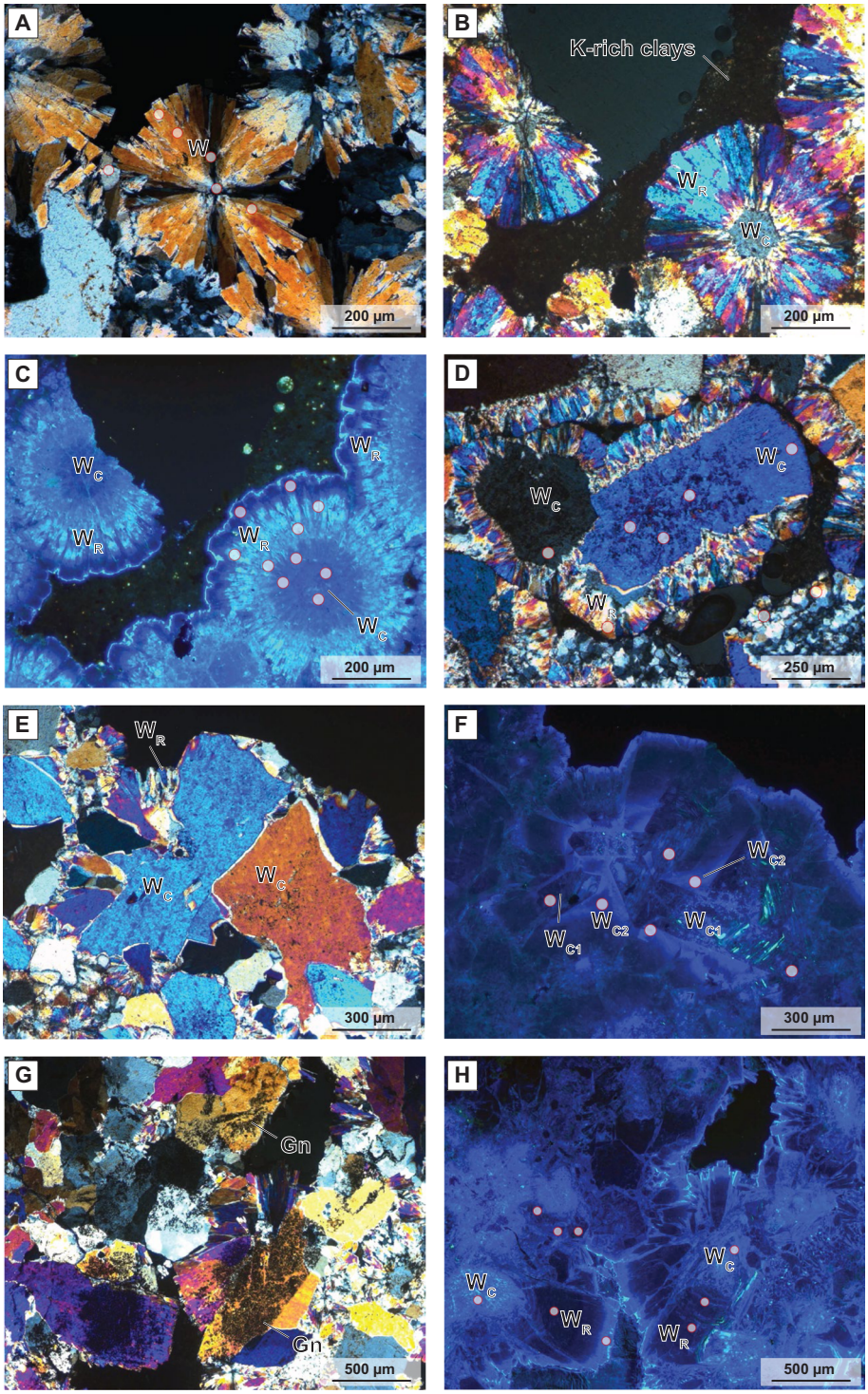

Fig. 2. Photomicrographs of the willemite mineralisation. (A) Willemite spherulite (type *W*) showing radially distributed elongated prisms (sample RA5232, TL, nic+). (B) Willemite spherulite composed of a rim of elongated prisms (W_R) around a core (W_C) formed by hexagonal crystals (sample RA6661, TL, nic+). (C) Same view in CL mode, to illustrate oscillatory zoning in the W_R. (D) Prismatic remnant core (W_C) of willemite rimmed by sub-fibrous willemite crystals (W_R) (sample RN3874, TL, nic+). (E) Aggregate of anhedral crystals of willemite (type W_C) coated by fibrous willemite crystals (W_R) (sample RN3874, TL, nic+). (F) Same view in CL mode, to reveal the presence of idiomorphic crystal relics within cores. (G) Well-developed elongated crystals spotted by black inclusions of Pb-bearing minerals like galena (Gn), which delineate growth banding (sample RA5232, TL, nic+). (H) Same view in CL mode, to illustrate irregular zoning in the W_R type. TL, transmitted light; CL, cathodoluminescence; nic+, crossed nicols. Red spots correspond to the location of LA-ICPMS analyses.

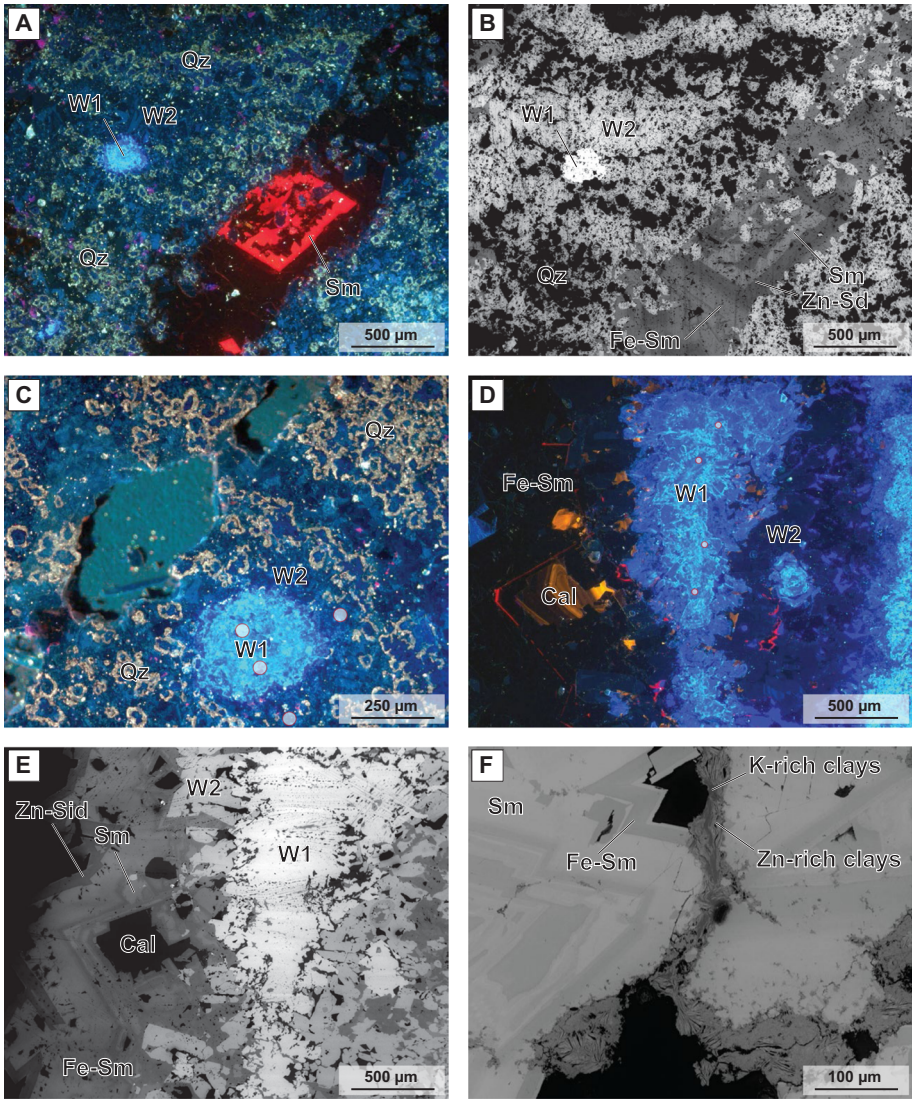

Fig. 3. Photomicrographs of the willemite mineralisation. (A) Relics of early willemite (W_1) embedded in a mixture of late willemite (W_2) and zoned quartz (Qz); willemite mineralisation is crosscut by a vein of carbonates showing red luminescence (sample IG32-105, CL). (B) Same view in BSE mode; note the difference in grey tone between the two willemite types and the composite nature of vein carbonates (Sm, smithsonite; Fe–Sm, Fe-rich smithsonite; Zn–Sd, Zn-rich siderite). (C) Details of the polyphase willemite mineralisation, and the core-mantle texture of quartz mixed with late willemite (sample IG32-105, CL). (D) Late willemite aggregates with relics of early willemite, coated by a complex late carbonate (Cal, calcite) stage (sample RN4019-105, CL). (E) Same view in BSE mode. (F) BSE image of zoned smithsonite formed in druses further filled with detrital K-rich clays (dark grey), partly replaced by zinc clays (light grey) (sample RN4019-105). BSE, Back-scattered electron.

the Ge content is below 3 ppm, while Ga and In are not detected.

5. Discussion

5.1. Polyphase willemite mineralization

Based on new observations of the non-sulphide ores, we propose the paragenetic succession presented in Fig. 6. As already noted by Coppola *et al*. (2008), three different mineralization stages can be distinguished. Whereas an early sulphide stage is locally preserved as massive sphalerite (Fig. 5A–E) or as tiny relics within silicates and carbonates (Fig. 2F–H), the non-sulphide mineralization includes two successive ore stages: (1) the willemite stage and (2) the carbonate stage. Dejonghe & Boni (2005) and Coppola *et al*. (2008) interpreted the various-scale associations of willemite and sphalerite as the result of a direct replacement process. However, our observations support a combination of dissolution and cementation, as shown by the presence of secondary sulphides (galena) that armour partly dissolved sphalerite and predate willemite precipitation (Fig. 4F). The relative incompatibility of lead within the willemite structure could also explain such textures (Terracciano, 2008). The transition between willemite and carbonate stages is characterized by: (1) direct replacement process

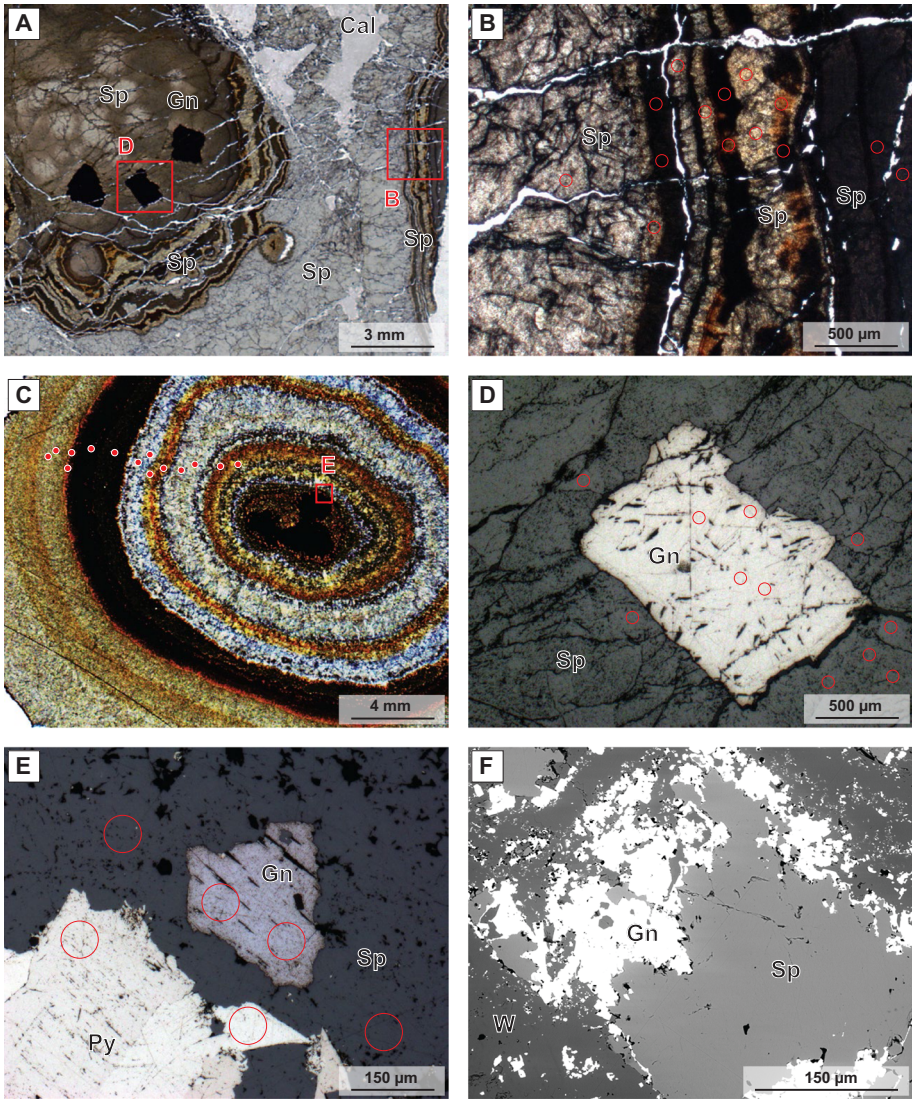

Fig. 4. Photomicrographs (plane-polarised light) of the sulphide mineralisation. (A) General view of the banded *schalenblende* spherulite cemented by colourless sphalerite and calcite (sample RN6483, TL). (B) Detailed view of banded sphalerite (sample RN6483, TL). (C): General view of banded *schalenblende* spherulite (sample RV2-837, TL). (D) Galena crystal included in sphalerite (sample RN6483, RL). (E) Sulphide (galena and pyrite) inclusions in the core of *schalenblende* spherulite (sample RV2-837, RL). (F) Secondary galena armouring relics of sphalerite within the non-sulphide mineralisation (sample RA5232, BSE). RL, reflected light.

(Dejonghe & Boni, 2005), (2) partial dissolution of willemite followed by carbonate precipitation (*e.g.*, Fig. 3) and (3) carbonates filling veins in willemite (Coppola *et al.*, 2008).

The coexistence of willemite and carbonate stages in a given mineralization is frequently reported in supergene Zn deposits (Terracciano, 2008; Choulet *et al.*, 2017; Mondillo *et al.*, 2018b). While the late mineral assemblage, including smithsonite, cerussite, hemimorphite, and hydrozincite, clearly indicates supergene weathering, the origin of the willemite stage in non-sulphide deposits has always been a matter of debate. On the basis of fluid-inclusion studies (*e.g.*, Sweeney *et al.*, 1991; Kamona & Friedrich, 2007; Terracciano, 2008), it is now widely accepted that willemite may also originate from hydrothermal-hypogene processes (Hitzman *et al.*, 2003). In this case, the precipitation of willemite from mid to-high salinity hydrothermal fluids may occur under: (1) oxidized conditions, (2) low sulfur activity, (3) moderate temperature (100–150 °C) and (4) pH > 6.5 (Brugger *et al.*, 2003). Many Neoproterozoic to Cambrian willemite deposits from the southern hemisphere formed by such hypogene processes, *e.g.*, Vazante in Brazil (Monteiro *et al.*, 2007; Slezak *et al.*, 2014), Zambezi prospects in Zambia (Terracciano, 2008; Boni *et al.*, 2011) or Beltana in Australia (Groves *et al.*, 2003). However, in several other deposits, such hypogene features are lacking, as exemplified by the willemite mineralization in Belgium (Coppola *et al.*, 2008). Although two-phase fluid inclusions in willemite provided homogenization temperatures between 80 °C and 190 °C (Boni *et al.*, 2005), monophase inclusions are predominant, suggesting that low temperature (50–80 °C) fluids have caused the precipitation of willemite. Coppola *et al.* (2008) considered that the high temperature obtained from two-phase inclusions is rather due to post-entrapment

Table 2. Major (EPMA, in wt%) and trace (LA-ICPMS, in ppm) element composition of willemite. < d.l.: maximum value lower than detection limit (see Materials and Methods section for d.l. calculation).

Type	*n*	SiO_2	ZnO	FeO	CaO	Mg	Al	P	Ti	Mn	Cu	Ga	Ge	As	Ag	Cd	Sn	Sb	Pb
		wt%				ppm													
W_1	66																		
	Mean	27.7	72.4	0.1	0.0	71	289	1006	23	61	2.0	0.3	40	138	1.0	8.1	0.4	1.0	1367
	Min	26.3	70.3	0.0	0.0	0.2	2.2	7.0	2.6	1.2	<d.l.	<d.l.	<d.l.	1.4	<d.l.	4.1	<d.l.	<d.l.	12
	Max	29.2	73.8	0.7	0.4	1910	2030	4110	251	1460	7.6	1.1	247	1195	26	19	2.0	13	7780
W_{1b}	4																		
	Mean					3.4	5.9	510	2.9	3.5	8.2	0.1	52	238	27	4.2	0.2	75	65175
	Min					0.7	2.4	139	1.7	2.3	5.4	<d.l.	8.8	177	22	3.6	<d.l.	23	27800
	Max					4.6	9.2	1335	3.9	4.5	14	1.0	167	304	32	4.9	1.0	134	86700
W_C	44																		
	Mean	27.6	72.5	0.2	0.0	364	3255	1909	87	76	2.5	1.0	37	354	0.6	14	0.8	0.8	413
	Min	26.1	69.9	0.0	0.0	18	25	395	5.3	4.1	<d.l.	<d.l.	5.2	24	<d.l.	3.0	<d.l.	<d.l.	102
	Max	28.7	73.5	2.0	0.1	1647	23800	3940	382	493	7.0	4.1	252	1466	2.3	30	2.7	2.7	1034
W_{C1}	4																		
	Mean	28.0	73.1	0.1	0.0	25.5	146	263	12	13	2.8	0.1	24	29	0.4	4.8	0.3	0.4	648
	Min	27.7	72.7	0.0	0.0	6.9	31	76	4.5	2.8	<d.l.	<d.l.	7.0	19	<d.l.	4.3	<d.l.	<d.l.	302
	Max	28.2	73.5	0.2	0.0	69	367	500	27	20	9.3	1.0	37	48	0.5	5.3	1.0	0.6	916
W_{C2}	4																		
	Mean	27.7	73.3	0.0	0.0	24	214	1411	20	2.0	0.8	0.1	68	127	0.6	4.5	0.4	1.9	494
	Min	27.4	73.1	0.0	0.0	2.2	5.0	337	7.7	1.1	<d.l.	<d.l.	20	43	<d.l.	4.3	<d.l.	0.5	238
	Max	28.1	73.6	0.1	0.0	85	801	1868	34	2.9	1.5	1.0	104	174	0.9	4.7	1.0	2.6	677
W_R	38																		
	Mean	27.8	72.6	0.1	0.0	190	1369	666	45	50	1.6	0.7	22	461	0.6	12	0.7	1.2	413
	Min	26.9	70.9	0.0	0.0	5.8	134	<d.l.	7.2	4.2	<d.l.	<d.l.	2.8	87	<d.l.	4.5	<d.l.	<d.l.	67
	Max	28.7	73.8	0.5	0.1	1864	7620	2170	290	921	7.7	1.9	99	3867	2.9	33	2.1	3.1	1251
W_2	9																		
	Mean	27.9	74.1	0.2	0.0	36	148	772	8.5	12	2.4	0.1	17	5.1	1.0	47	0.7	–	23
	Min	24.9	72.8	0.0	0.0	1.2	0.8	99	3.5	<d.l.	<d.l.	<d.l.	1.0	d.l.	d.l.	26	<d.l.	<d.l.	2.1
	Max	30.2	76.4	0.5	0.0	211	311	2237	20	41	9.2	1.0	59	16	2.8	61	1.2	<d.l.	104

Table 3. Major (EPMA) element composition in wt% of carbonates. *SD* is for standard deviation.

	Smithsonite (*n* = 9)				Fe-rich smithsonite (*n* = 19)				Zn-rich siderite (*n* = 6)			
	Mean	*SD*	Min	Max	Mean	*SD*	Min	Max	Mean	*SD*	Min	Max
MgO	2.0	1.9	0.1	5.6	3.5	1.2	1.4	5.1	2.6	0.9	1.6	3.8
MnO	0.4	0.5	0.0	1.3	1.1	1.0	0.1	2.9	0.8	0.5	0.1	1.7
FeO	0.9	1.0	0.0	3.1	15.5	5.9	9.0	27.5	43.7	1.8	41.6	47.0
CdO	0.0	0.0	0.0	0.1	0.0	0.0	0.0	0.0	0.0	0.0	0.0	0.0
CaO	0.5	0.4	0.0	1.1	1.1	0.6	0.1	1.8	4.6	0.6	3.8	5.4
ZnO	61.5	4.1	57.5	66.6	41.5	7.7	27.0	51.7	6.9	2.0	3.9	9.4
CO_2*	36.9	1.1	35.7	39.4	37.5	1.0	35.7	39.2	38.0	0.3	37.7	38.5
Total	102.0	1.1	100.4	103.6	100.1	1.3	97.9	103.3	96.6	0.8	95.6	97.8

*Calculated from stoichiometry.

modifications than to primary hypogene process. Therefore, it is not possible to distinguish between low-temperature hydrothermal processes and a strict supergene origin for willemite mineralization.

This study also reveals the polyphase nature of willemite ores from the historical deposits of Eastern Belgium. Following previous studies, which reported idiomorphic crystals with hexagonal habits and botryoidal aggregates showing acicular radiated crystals (Boni *et al*, 2005; Coppola *et al*., 2008), two successive types, namely W_R and W_C are distinguished. We also noted that these two types have themselves recorded a complex evolution (*e.g*., W_{C1} and W_{C2}; Fig. 6). Although all these willemite types have distinct morphological and internal zoning features, they are chemically similar (Table 2). Following a botryoidal stage, we also noted the precipitation of late willemite (W_2), whose mineral chemistry significantly differs from those of other types. The latter occurs as a cement between early spherules and aggregates (W_1), but predates the formation of zinc carbonates (Fig. 3C–E). Its precipitation is also texturally associated with the development of quartz rims around pre-existing quartz (Fig. 6).

The polyphase nature of willemite mineralization was also described in several other deposits throughout the world. In the Bou Arhous deposit in Morocco, several morphological types of willemite are reported, but only two separate

Table 4. Major (EPMA) and trace (LA-ICPMS) element composition of sphalerite. <d.l.: Maximum value lower than detection limit (see Materials and Methods section for d.l. calculation).

Sample		Zn	S	Fe		Co	Ni	Cu	Ga	Ge	As	Ag	Cd	Sn	Sb	Pb
		wt%				ppm										
RV2-837	n = 17				n = 16											
	Mean	66.8	32.1	0.7		0.5	9.1	1.1	0.1	269	667	3.3	2381	0.2	77	1805
	Min	63.2	31.2	0.1		<d.l.	5.9	<d.l.	<d.l.	20	55	<d.l.	414	<d.l.	<d.l.	479
	Max	68.6	32.7	3.6		1.6	15	10	0.8	521	2230	20	8930	1.0	497	3926
RN6483	n = 23				n = 26											
	Mean	65.8	31.9	1.1		0.5	1.9	4.8	0.6	246	417	1.6	593	0.3	15	1874
	Min	38.7	23.3	0.0		<d.l.	<d.l.	<d.l.	<d.l.	19	1.1	0.4	58	<d.l.	0.8	36
	Max	69.1	32.8	5.7		1.7	3.4	27	3.2	1325	4540	13	2109	1.0	70	10060

generations were clearly distinguished, based on the presence of an intermediate dissolution stage (Choulet *et al.*, 2017). In Namibian Berg-Aukas type Zn deposits (Misiewicz, 1988), up to three successive stages of willemite are distinguished, especially by the different cathodoluminescence colours (Terracciano, 2008). No difference of major-element chemistry between willemite generations is observed, and no trace-elements analysis is currently available (Terracciano, 2008). Willemite is considered to have precipitated from low-T hydrothermal fluids and predates a later strictly supergene carbonate stage. In the Kabwe deposit in Zambia, the two successive willemite generations are also reported. While Kamona & Friedrich (2007) have proposed an early hypogene stage followed by supergene stage, Terracciano (2008) proposed that willemite is of supergene or low-T hydrothermal origin. Recent oxygen isotopic data obtained by Mondillo *et al.* (2018b) support that both generations of willemite and the late carbonates are not cogenetic in the Kabwe ores, ruling out a strictly supergene scenario for willemite precipitation.

Although we cannot distinguish between low-T hydrothermal and supergene origin for willemite in the Belgian deposits, all microscopic observations support that all willemite types, except W_2, are part of a single continuous stage. The differences in trace-element composition (Table 2) could reflect either a local source effect, impurities or a progressive change of composition for the mineralizing fluid. Such a change was observed in the willemites from Bou Arhous (Choulet *et al.*, 2017) and Tres Marias (Saini-Eidukat *et al.*, 2009), since oscillatory zoning is associated with changes of minor and trace elements composition.

5.2. Link between compositions of willemite and protore minerals

In situ measurements by LA-ICPMS revealed a significant amount of trace elements incorporated in willemite. Among them, high Pb content is correlated with other metal enrichment (especially Ag) but not with Zn content, suggesting that nano to micro-inclusions of Pb-rich minerals occur within willemite (Fig. 2G and H). A similar interpretation was proposed for the W_1 willemite from Kabwe (Mondillo *et al.*, 2018b). Conversely, high Pb contents (up to 2 wt%) were measured in willemite from Bou Arhous, Morocco (Choulet *et al.*, 2017) and Tres Marias, Mexico (Saini-Eidukat *et al.*, 2009). In both cases, there is a strong negative correlation between Zn and Pb, suggesting that Pb substitutes for Zn in the willemite structure. This is confirmed by XANES spectrometry, which shows that Pb is present as eightfold-coordinated Pb^{2+} in agreement with a lattice substitution model (Saini-Eidukat *et al.*, 2016).

Arsenic and phosphorous also occur in variable amounts within willemite (up to 3867 ppm and 3940 ppm, respectively). The concentration of As is higher than previously reported for willemite from Belgium (Coppola *et al.*, 2008). Such enrichments were reported for Tres Marias willemite with up to 0.76 wt% P_2O_5 and 0.8 wt% As_2O_3 contents (Saini-Eidukat *et al.*, 2009). In addition, these elements display heterogeneous distribution and can be used to discriminate between the willemite types with different morphological features. While the As contents generally average several hundred ppm in most willemite types (Table 2), very low As contents (less than 60 ppm) are measured in inherited core crystals (W_{C1}) and in late willemite crystals (W_2). Significant differences in As content are also reported between the two willemite generations from the Kabwe deposit (Mondillo *et al.*, 2018b). Further investigation of the P and As contents and their distribution could be used as geochemical fingerprints in order to better understand the nature of fluids involved in willemite mineralization.

The cadmium content differs between early (means ranging from 4 ppm to 14 ppm) and late generations of willemite (mean 47 ppm for W_2; Table 2). The latter value is consistent with the average values reported from Kabwe willemite (means 40–71 ppm; Mondillo *et al.*, 2018b). Indium concentrations are below detection limit, as measured for Kabwe willemite (Mondillo *et al.*, 2018b). The Ga content is lower than 4 ppm (Table 2), showing values significantly lower than those reported from the Kabwe deposit (up to 28 ppm; Mondillo *et al.*, 2018b). Despite the absence of obvious correlation between Ga and Al at Kabwe, both elements are positively correlated in samples from Belgium. This could reflect a contamination of several analyses by Al-rich phases (*e.g.*, clay minerals), which are commonly reported either as inclusion or as secondary products after willemite (*e.g.*, Choulet *et al.*, 2016). The Ge contents range between the detection limit and 250 ppm, with means of several tens of ppm depending on the willemite

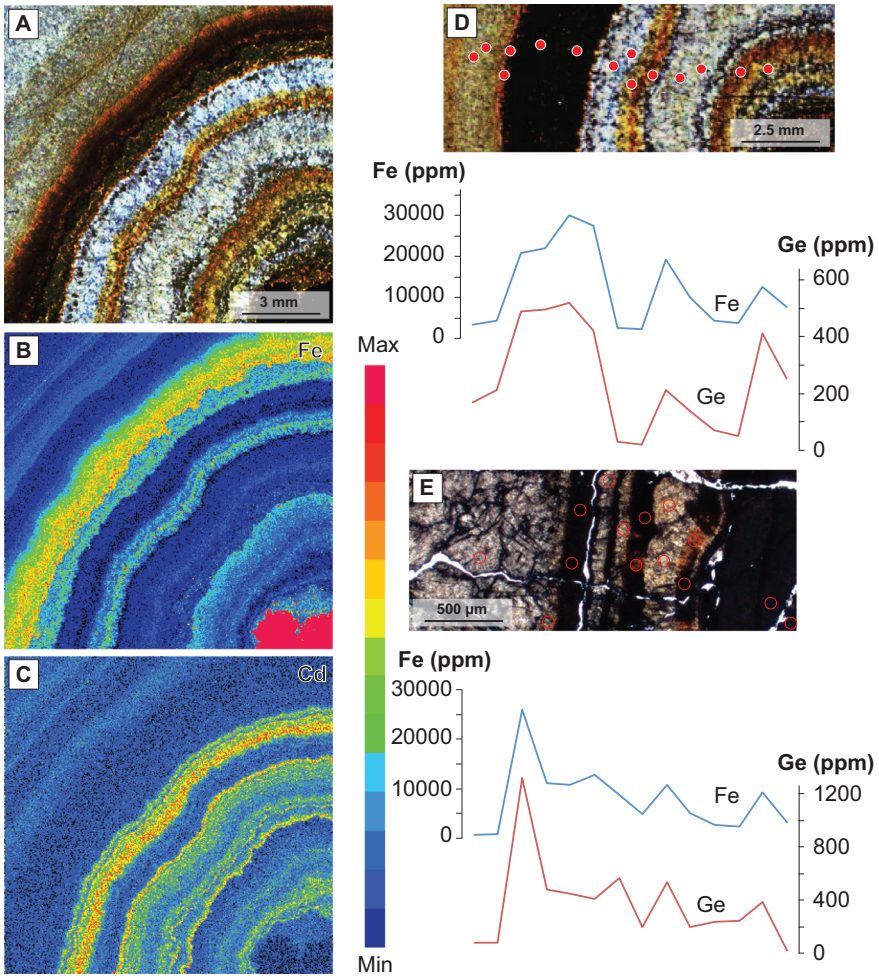

Fig. 5. Elementary composition of sphalerite. (A–C) Chemical mapping (Cd and Fe) by EPMA of banded *schalenblende* spherulite with a pyrite inclusion in the core; note the first-order inverse correlation between Cd and Fe. (D and E) Elementary profiles, based on LA-ICPMS data, across banded sphalerite to illustrate the correlation between Fe and Ge domains.

type. However, except for the low Ge contents in late willemite stage W_2, no significant differences in Ge content are observed between other willemite types (Table 2). Means of several tens of ppm of Ge were also measured in Kabwe willemite (Mondillo *et al*., 2018b), and in several willemite crystals from supergene deposits of New Mexico and Utah (Sheffer, 1966). As these values are significantly higher than the content measured in hypogene willemite from Franklin (<10 ppm; Sheffer, 1966), it is significantly lower than in several localities throughout the world, such as Tsumeb in Namibia (up to 1280 ppm; Lombaard *et al*., 1986) and Tres Marias in Mexico (4000 ppm; Saini-Eidukat *et al*., 2009). Such high Ge contents in willemite are explained by incorporation of Ge^{4+} within the silica tetrahedra (Saini-Eidukat *et al*., 2016). Choulet *et al*. (2017) also reported Ge contents up to 1100 ppm in willemite from the Bou Arhous deposits. Interestingly, in the latter case, the content is highly heterogeneous and depends on the willemite type, defined by sector and oscillatory zoning (Choulet *et al*., 2017). In the case of Belgian deposits, we do not observe sector zoning like in Morocco. Together with oscillatory zoning, core and rim textures are frequently observed (Fig. 2), but the Ge content does not differ between the various morphological and zoning features. Crystallographic controls on trace-element composition are therefore limited to particular textures, as also observed for a range of minerals (Reeder & Rakovan, 1999), *e.g*., sphalerite (Belissont *et al*., 2014) or pyrite (Chouinard *et al*., 2005).

In addition to crystal surface structure (*e.g*., Reeder & Rakovan, 1999) and kinetics effects (*e.g*., Putnis, 2009), the trace-element contents of willemite are directly influenced by the nature of mineralizing fluids and the initial contents of mineral phases predating willemite. The germanium concentrations are generally low (<0.1 ppb) in surface water (*e.g*., Höll *et al*., 2007). In thermal water, this concentration can reach up to 100 ppb (*e.g*., Kraynov, 1967; Simmons *et al*., 2018). Germanium is transported as hydroxide and chloro-complexes (Pokrovski & Schott, 1998). Although the Ge content of fluids increases with temperature (Bernstein, 1985), hypogene willemite from Franklin has low Ge content (10 ppm; Sheffer, 1966). At Kabwe, early willemite probably formed by hypogene processes is depleted in Ge compared to the late willemite derived from either hydrothermal or supergene processes (Mondillo *et al*.,

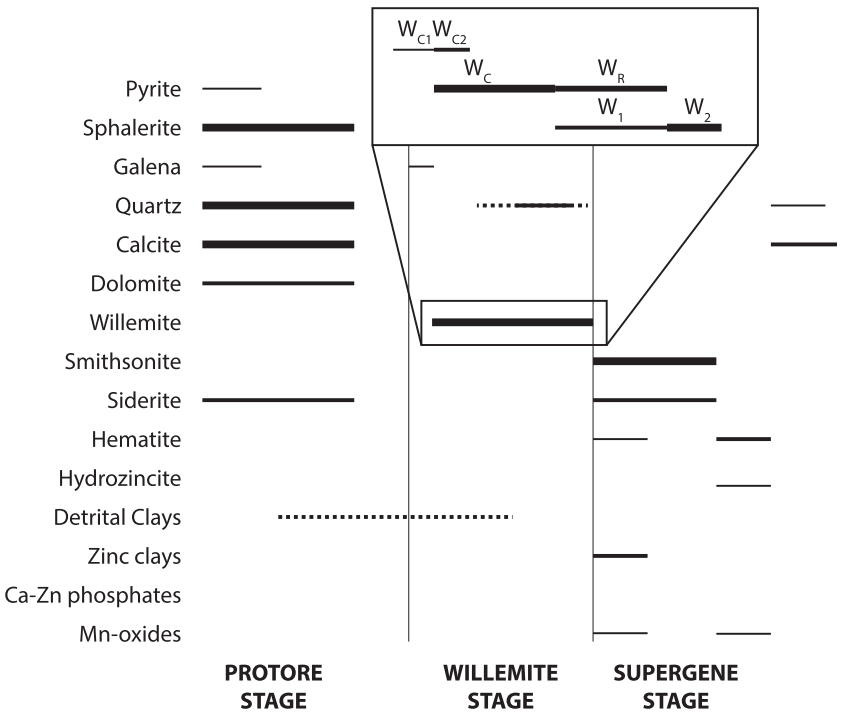

Fig. 6. Summary paragenetic sequence of the observed and inferred (from Coppola *et al.*, 2008) minerals in the non-sulphide mineralisation of eastern Belgium. Insert is a detailed view of the willemite types reported in the samples. See text for explanation of willemite typology. Thickness of the horizontal line corresponds to the relative abundance of each mineral species.

2018b). This suggests that the geochemistry of the mineralizing fluid has only a very limited influence on the trace-element content of willemite formed by supergene or hydrothermal processes.

As reported in many studies, willemite occurs as a replacement of primary sphalerite (Sweeney *et al.*, 1991; Coppola *et al.*, 2008; Terracciano, 2008; Saini-Eidukat *et al.*, 2009). Sphalerite is known for hosting a large range of trace elements (Cook *et al.*, 2009), including germanium or gallium. In general, a Ga–Ge-enriched group is distinguished from a Fe–Mn–In group and corresponds to low-temperature deposits, such as MVT deposits (Belissont *et al.*, 2014; Frenzel *et al.*, 2016). High concentrations of Ge up to several thousands ppm have been reported in samples from Tres Marias (max. 1320 ppm; Saini-Eidukat *et al.*, 2009), Saint-Salvy (max. 2576 ppm; Belissont *et al.*, 2014) or Kipushi (5930 ppm; Belissont, 2016), but a correlated Ga enrichment is not always reported (*e.g.*, Cook *et al.*, 2009; Ye *et al.*, 2011). In sphalerite from Belgium, the Ge content ranges from 19 ppm to 1325 ppm with averages at 270 ppm and 250 ppm, depending on samples (Table 4). The Ga content is lower than 3 ppm; these values are consistent with previously published results from sphalerite collected in eastern Belgium, with means for Ge and Ga at 302 ppm and 2.2 ppm, respectively (Goffin *et al.*, 2015). Other sulphides (galena and pyrite) carry very low Ge and Ga contents (Duchesne *et al.*, 1983). As already pointed out by Goffin *et al.* (2015), the Ge concentration in sphalerite increases with iron content (Fig. 5). Such trend is also observed in sphalerites from the Tres Marias MVT deposit (Saini-Eidukat *et al.*, 2009), suggesting the following substitution $2Fe^{2+} + Ge^{4+} + \square \leftrightarrow 4Zn^{2+}$ ($\square$ for vacancy; Cook *et al.*, 2009, 2015). This trend is quite unusual because Ge (and Ga) enrichment generally occurs in Fe-poor bands or sectors in MVT deposits (Cook *et al.*, 2009; Belissont *et al.*, 2014; Frenzel *et al.*, 2016). The Ge contents in willemite and sphalerite are of the same order (Tables 2 and 4). This is very similar to Ge-poor deposits such as Kabwe (3–91 ppm for willemite; 1–31 ppm for sphalerite; Mondillo *et al.*, 2018b), or Ge-rich deposits at Tres Marias (up to 4000 ppm for willemite; up to 1320 ppm for sphalerite; Saini-Eidukat *et al.*, 2009). This further indicates that the composition of primary sphalerite has a crucial role in the final Ge (and Ga) content of willemite. However, some exceptions are also reported, *e.g.*, Ge-rich (up to 1100 ppm) willemite replacing Ge-poor sphalerite (<100 ppm) at Bou Arhous (Choulet *et al.*, 2017). In this case, such a difference can be explained rather by selective incorporation of Ge in particular faces of the willemite crystals than by an external supply from Ge-rich hydrothermal fluids, which are extremely rare even in sulphide-rich mine waters (Goleva & Vorobyeva, 1967).

An alternative control for trace-element enrichment in a mineral phase is the competition with other minerals formed earlier or synchronously. In all willemite-bearing deposits, willemite is always the first mineral to be formed after the protore stage. In some rare cases, it can be preceded by secondary sulphides (galena, greenockite, covellite), which can

armour sphalerite (Fig. 4F) and trigger minor elements such as Cd into greenockite (Choulet *et al*., 2014). Other mineral phases may co-precipitate in the oxidation zone and serve as potential hosts for trace elements and particularly Ge (Höll *et al*., 2007). In the oxidized ore of the Tsumeb deposit, willemite occurs together with numerous secondary minerals such as Ge oxides and Ge hydroxides (Lombaard *et al*., 1986; Melcher, 2003). At Tsumeb, iron hydroxides and various arsenates can also incorporate large amounts of Ge (up to 2.5 wt% in Melcher, 2003), limiting Ge content within willemite to 1280 ppm (Lombaard *et al*., 1986). Such competition between mineral phases is also illustrated in the supergene Cristal non-sulphide prospect in Peru, where Ge, initially present in sphalerite (mean at 140 ppm), is distributed between goethite (means between 100 ppm and 230 ppm) and hemimorphite (means between 40 ppm and 140 ppm) (Mondillo *et al*., 2018a). The incorporation of Ge in the minerals of the carbonate stage is limited to few ppm, though, as exemplified by low Ge contents in supergene smithsonite from Jbel Haounit, eastern Morocco (Verhaert *et al*., 2017). Such secondary distribution has important implication either for exploration of unconventional Ge targets or for optimized mineral processing to recover germanium.

6. Conclusion

This study presents new observations and chemical analyses of willemite mineralization from the historical "Calamine-type" deposits of eastern Belgium. Willemite occurs as a variety of types that continuously formed between the protore stage (sulphides) and the supergene stage (carbonates and hydrated phases). While the different types of willemite may be distinguished by their shape and zoning characteristics, changes of composition are slight, except for the late type, which probably represents a separate and later generation. Among trace elements, Ge contents up to 250 ppm are measured, consistent with other values reported from willemite mineralization throughout the world. Concentrations obtained in willemite are similar to those measured in sphalerite (ranging between 19 ppm and 1325 ppm, mean at 250 ppm).

Based on these results, we conclude that the non-sulphide zone of ore deposits has a real potential for exploration of minor metals and especially Ge. However, several features should be taken into account:

- The extent of the alteration/weathering zone itself depends on climate and tectonic factors, which control its development and its preservation through time;
- Ge enrichment is accompanied by a range of other minor elements (As, P, Cd, Pb), which may have a negative impact either on environmental issues or recovery process;
- willemite mineralization often occurs as a variety of forms, exposing variations of trace-element composition. The latter can change due to (1) the initial content of sulphide precursors, (2) the addition of metals by external fluids (hydrothermal or supergene), (3) a competition between willemite and other phases [especially iron (hydr-)oxides] for hosting trace elements, and (4) fractionation within mineral phases with selective incorporation in the crystal structure.

Acknowledgements: Thanks are due to Marleen De Ceukelaire for assistance during sampling at the Royal Belgian Institute of Natural Sciences (Brussels). This work was partly associated to the project « Révision de la Carte géologique de Wallonie » of the Geological Survey of Wallonia (Service Public de Wallonie). The authors also warmly acknowledge the assistance of Didier Convert-Gaubier (Chrono-Environment, Besançon) for thin-section preparation and Martin Robyr (Université de Lausanne) for EPMA data acquisition. This study has benefited from financial support by INSU-CESSUR 2016 programme. Research activity of Marie-Christine Boiron is supported by the French National Research Agency through the ''Investissements d'avenir" programme, reference ANR-10-LABX-21-LABEX. Access to SEM facilities of the MIMENTO centre was made in the frame of cooperative projects in the Renatech network. This paper has benefited from the careful handling and reviews of Patrick Cordier (Editor-in-Chief), Allan Pring (Associate Editor), Franck Melcher (reviewer) and an anonymous reviewer.

References

Belanger, I., Delaby, S., Delcambre, B., Ghysel, P., Hennebert, M., Laloux, M., Marion, J.-L., Mottequin, B., Pingot, J.-L. (2012): Redéfinition des unités structurales du front varisque utilisées dans le cadre de la nouvelle Carte géologique de Wallonie (Belgique). *Geol. Belg.*, **15**, 169–175.

Belissont, R. (2016): Germanium and related elements in sulphide minerals: crystal chemistry, incorporation and isotope fractionation. PhD Dissertation, Université de Lorraine, Nancy, France, 210 p.

Belissont, R., Boiron, M.-C., Luais, B., Cathelineau, M. (2014): LA-ICP-MS analyses of minor and trace elements and bulk Ge isotopes in zoned Ge-rich sphalerites from the Noailhac–Saint-Salvy deposit (France): insights into incorporation mechanisms and ore deposition processes. *Geochim. Cosmochim. Acta*, **126**, 518–540.

Belissont, R., Munoz, M., Boiron, M.C., Luais, B., Mathon, O. (2016): Distribution and oxidation state of Ge, Cu and Fe in sphalerite by μ-XRF and K-edge μ-XANES: insights into Ge incorporation, partitioning and isotopic fractionation. *Geochim. Cosmochim. Acta*, **177**, 298–314.

Bernstein, L.R. (1985): Germanium geochemistry and mineralogy. *Geochim. Cosmochim. Acta*, **49**, 2409–2422.

— (1986): Geology and mineralogy of the APEX germanium–gallium mine, Washington County, Utah. *USGS Bull.*, **1577**, 1–9.

Boni, M. & Mondillo, N. (2015): The "Calamines" and the "Others": the great family of supergene nonsulfide zinc ores. *Ore Geol. Rev.*, **67**, 208–233.

Boni, M., Coppola, V., Dejonghe, L., Fedele, L. (2005): Willemite in the Belgian nonsulfide zinc deposits: a fluid inclusion study. *Period. Mineral.*, **74**, 87–100.

Boni, M., Gilg, H.A., Aversa, G., Balassone, G. (2003): The "Calamine" of SW Sardinia (Italy): geology, mineralogy and

stable isotope geochemistry of a supergene Zn-mineralization. *Econ. Geol.*, **98**, 731–748.

Boni, M., Terracciano, R., Balassone, G., Gleeson, S.A., Matthews, A. (2011): The carbonate-hosted willemite prospects of the Zambezi Metamorphic Belt (Zambia). *Mineral. Deposita*, **46**, 707–729.

Borg, G. (2009): The role of fault structures and deep oxidation in supergene base metal deposits. *in* "Supergene environments, processes and products", S.R. Titley, ed., *Econ. Geol. Spec. Publ.,* **14**, 121–132.

Brugger, J., McPhail, D.C., Wallace, M., Waters, J. (2003): Formation of willemite in hydrothermal environments. *Econ. Geol.*, **8**, 919–935.

Cesàro, G. (1887): Note sur quelques minéraux (dont la willémite fibroradiée de Moresnet). *Ann. Soc. Géol. Belg.*, **14**, 142–143.

Chouinard, A., Paquette, J., Williams-Jones, A.E. (2005): Crystallographic controls on trace-element incorporation in auriferous pyrite from the Pascua epithermal high-sulfidation deposit, Chile-Argentina. *Can. Mineral.*, **43**, 951–963.

Choulet, F., Charles, N., Barbanson, L., Branquet, Y., Sizaret, S., Ennaciri, A., Badra, L., Chen, Y. (2014): Non-sulfide zinc deposits of the Moroccan High Atlas: multi-scale characterization and origin. *Ore Geol. Rev.*, **56**, 115–140.

Choulet, F., Buatier, M., Barbanson, L., Guégan, R., Ennaciri, A. (2016): Zinc-rich clays in supergene non-sulfide zinc deposits. *Mineral. Deposita*, **51**, 467–490.

Choulet, F., Barbanson, L., Buatier, M., Richard, J., Vennemann, T., Ennaciri, A., Zouhair, M. (2017): Characterization and origin of low-T willemite (Zn_2SiO_4) mineralization: the case of the Bou Arhous deposit (High Atlas, Morocco). *Mineral. Deposita*, **52**, 1085–1102.

Cook, N.J., Ciobanu, C.L., Pring, A., Skinner, W., Danyushevsky, L., Shimizu, M., Saini- Eidukat, B., Melcher, F. (2009): Trace and minor elements in sphalerite: a LA-ICP-MS study. *Geochim. Cosmochim. Acta*, **73**, 4761–4791.

Cook, N.J., Etschmann, B., Ciobanu, C.L., Geraki, K., Howard, D. L., Williams, T., Rae, N., Pring, A., Chen, G., Johannessen, B., Brugger, J. (2015): Distribution and substitution mechanism of Ge in Ge–(Fe)-bearing sphalerite. *Minerals*, **5**, 117–132.

Coppola, V., Boni, M., Gilg, H.A., Balassone, G., Dejonghe, L. (2008): The "Calamine" nonsulfide Zn–Pb deposits of Belgium: petrographical, mineralogical and geochemical characterization. *Ore Geol. Rev.*, **33**, 187–210.

Dejonghe, L. (1998): Zinc–lead deposits of Belgium. *Ore Geol. Rev.*, **12**, 329–354.

Dejonghe, L. & Boni, M. (2005): The "Calamine-type" zinc–lead deposits in Belgium and West Germany: a product of Mesozoic palaeoweathering processes. *Geol. Belg.*, **8–3**, 3–14.

Dejonghe, L. & Jans, D. (1983): Les gisements plombo-zincifères de l'Est de la Belgique. *Chron. Rech. Min.*, **470**, 3–24.

Dejonghe, L., Ladeuze, F., Jans, D. (1993): Atlas des gisements plombo-zincifères du Synclinorium de Verviers (Est de la Belgique). *Mém. Cartes Géol. Min. Belg.*, **33**, 1–483.

Demoulin, A., Barbier, F., Dekoninck, A., Verhaert, M., Ruffet, G., Dupuis, C., Yans, J. (2018): Erosion surfaces in the Ardenne–Oesling and their associated kaolinic weathering mantle. *in* "Landscapes and landforms of Belgium and Luxembourg". A. Demoulin, ed. Springer International Publishing, Cham, 63–84.

Drzazga, M., Prajsnar, R., Chmielarz, A., Benke, G., Leszczyńska-Sejda, K., Ciszewski, M., Bilewska, K., Krawiec, G. (2018): Germanium and indium recovery from zinc metallurgy by-products—dross leaching in sulphuric and oxalic acids. *Metals*, **8**, 1041.

Duchesne, J.-C., Rouhart, A., Schoumaker, C., Dillen, H. (1983): Thallium, nickel, cobalt, and other trace elements in iron sulphides from Belgian lead–zinc vein deposits. *Mineral. Deposita*, **18**, 303–313.

Fielitz, W. & Mansy, J.-L. (1999): Pre- and synorogenic burial metamorphism in the Ardenne and neighbouring areas (Rhenohercynian zone, central European Variscides). *Tectonophysics*, **309**, 227–256.

Franke, W. (2000): The mid-European segment of the Variscides: tectonostratigraphic units, terrane boundaries and plate tectonic evolution. *in* "Orogenic processes: quantification and modelling in the Variscan Belt", W. Franke, V. Haak, O. Oncken, D. Tanner, eds., Geological Society, Special Publications. Geological Society of London, London, 35–61.

Frenzel, M., Hirsch, T., Gutzmer, J. (2016): Gallium, germanium, indium, and other trace and minor elements in sphalerite as a function of deposit type — a meta-analysis. *Ore Geol. Rev.*, **76**, 52–78.

Goffin, V., Evrard, M., Pirard, E. (2015): Critical metals in sphalerites from Belgian MVT deposits. *in* "Proceedings of 13th SGA Biennial Meeting" **Vol. 2**, A.S. André-Mayer, M. Cathelineau, P. Muchez, E. Pirard & S. Sindern, eds., 24–27 August, Nancy, France, 741–744.

Goleva, G.A. & Vorobyeva, I.N. (1967): The migration of germanium in the ground waters of ore deposits. *Geochem. Int.*, **4**, 809–817.

Goossens, P.J. (2014): Zinc potential in Eastern Belgium. *Eur. Geol.*, **37**, 7–11.

Graulich, J.M., Dejonghe, L., Cnudde, C. (1984): La définition du Synclinorium de Verviers. *Bull. Soc. Belg. Géol.*, **93**, 79–82.

Groves, I., Carman, C.E., Dunlap, W.J. (2003): Geology of the Beltana willemite deposit, Flinders Ranges, South Australia. *Econ. Geol.*, **98**, 797–818.

Heijlen, W., Muchez, P., Banks, D.A. (2001): Origin and evolution of high-salinity, Zn–Pb mineralising fluids in the Variscides of Belgium. *Mineral. Deposita*, **36**, 165–176.

Hitzman, M.W., Reynolds, N.A., Sangster, D.F., Allen, C.R., Carman, C. (2003): Classification, genesis, and exploration guides for nonsulfide zinc deposits. *Econ. Geol.*, **98**, 685–714.

Höll, R., Kling, M., Schroll, E. (2007): Metallogenesis of germanium—a review. *Ore Geol. Rev.*, **30**, 145–180.

Kamona, A.F. & Friedrich, G.H. (2007): Geology, mineralogy and stable isotope geochemistry of the Kabwe carbonate-hosted Pb–Zn deposit, Central Zambia. *Ore Geol. Rev.*, **30**, 217–243.

Kraynov, S.R. (1967): Geochemistry of germanium in the thermal carbonate waters (illustrated by examples from the Pamirs and Greater Caucasus). *Geochem. Int.*, **4**, 309–320.

Lombaard, A.F., Günzel A., Innes J., Krüger T.L. (1986): The Tsumeb lead–copper–zinc–silver deposit, South West Africa/ Namibia. *in* "Mineral deposits of Southern Africa, Vol. 2", C.R. Anhaeusser & S. Maske, eds. Geological Society of South Africa, Johannesburg, 1761–1782.

Longerich, H.P., Jackson, S.E., Gunther, D. (1996): Laser ablation inductively coupled plasma mass spectrometric transient signal data acquisition and analyte concentration calculation. *J. Anal. Atom. Spectrom.*, **11**, 899–904.

Meilliez, F. & Mansy, J.-L. (1990): Déformation pelliculaire différenciée dans une série lithologique hétérogène: le Dévono-Carbonifère de l'Ardenne. *Bull. Soc. Géol. France*, **8–6**, 177–188.

Melcher, F. (2003): The Otavi Mountain Land in Namibia: Tsumeb, germanium and snowball earth. *Mitt. Österreich. Mineral. Gesell.*, **148**, 413–435.

Michot, P. (1980): Le segment tectogénique calédonien belge. *Mém. Classe Sci. Acad. R. Belg.*, **1890**, 1–61.

Misiewicz, J.E. (1988): The geology and metallogeny of the Otavi Mountain Land, Damara Orogen, SWA/Namibia, with particular reference to the Berg Aukas Zn-Pb-V deposit – a model of ore genesis. MSc Thesis, Rhodes University, Grahamstown, ZA, 143 p.

Mondillo, N., Arfè, G., Herrington, R., Boni, M., Wilkinson, C., Mormone, A. (2018a): Germanium enrichment in supergene settings: evidence from the Cristal nonsulfide Zn prospect, Bongará district, northern Peru. *Mineral. Depos.*, **53**, 155–169.

Mondillo, N., Herrington, R., Boyce, A.J., Wilkinson, C., Santoro, C., Rumsey, M. (2018b): Critical elements in non-sulfide Zn deposits: a reanalysis of the Kabwe Zn-Pb ores (central Zambia). *Mineral. Mag.*, **82**, S89–S114.

Monteiro, L.V.S., Bettencourt, J.S., Juliani, C., Oliveira, T.F. (2007): Non-sulfide and sulfiderich zinc mineralizations in the Vazante, Ambrosia and Fagundes deposits, Minas Gerais, Brazil: mass balance and stable isotope characteristics of the hydrothermal alterations. *Gondwana Res.*, **11**, 362–381.

Muchez, P., Slobodnik, M., Viaene, W., Keppens, E. (1994): Mississippi Valley-type Pb–Zn mineralization in Eastern Belgium: indications for gravity-driven flow. *Geology*, **22**, 1011–1014.

Muchez, P., Heijlen, W., Banks, D., Blundell, C., Boni, M., Grandia, F. (2005): Extensional tectonics and the timing and formation of basin-hosted deposits in Europe. *Ore Geol. Rev.*, **27**, 241–267.

Oncken, O., von Winterfeld, C., Dittmar, U. (1999): Accretion of a rifted passive margin: the Late Paleozoic Rhenohercynian fold and thrust belt (Middle European Variscides). *Tectonics*, **18**, 75–91.

Paton, C., Hellstrom, J., Paul, B., Woodhead, J., Hergt, J. (2011): Iolite: freeware for the visualisation and processing of mass spectrometric data. *J. Anal. Atom. Spectr.*, **26**, 2508. doi: 10.1039/c1ja10172b.

Pearce, N.J.G., Perking, W.T., Westgate, J.A., Gorton, M.P., Jackson, S.E., Neal, C.R., Chenery, S.P. (1997): A compilation of new and published major and trace element data for NIST SRM610 and NIST SRM612 glass materials. *Geostand. Newslett.*, **21**, 115–144.

Pokrovski, G.S. & Schott, J. (1998): Thermodynamic properties of aqueous Ge (IV) hydroxide complexes from 25 to 350 °C: implications for the behaviour of germanium and the Ge/Si ratio in hydrothermal fluids. *Geochim. Cosmochim. Acta*, **62**, 1631–1642.

Putnis, A. (2009): Mineral replacement reactions. *Rev. Mineral. Geochem.*, **70**, 87–124.

Quesnel, F. (2003): Paleoweathering and paleosurfaces from northern and eastern France to Belgium and Luxembourg: geometry, dating and geodynamic implications. *Géol. Fr.*, **1**, 95–104.

Reeder, R.J. & Rakovan, J. (1999): Surface structural controls on trace element incorporation during crystal growth. *in* "Growth, dissolution and pattern formation in geosystems", B. Jamtveit & P. Meakin, eds. Springer, Dordrecht, 143–162.

Reich, M. & Vasconcelos, P.M. (2015): Geological and economic significance of supergene metal deposits. *Elements*, **11**, 305–310.

Saini-Eidukat, B., Melcher, F., Lodziak, J. (2009): Zinc-germanium ores of the Tres Marias Mine, Chihuahua, Mexico. *Mineral. Deposita,* **44**, 363–370.

Saini-Eidukat, B., Melcher, F., Göttlicher, J., Steininger, R. (2016): Chemical environment of unusually Ge- and Pb-rich willemite, Tres Marias Mine, Mexico. *Minerals*, **6**, 20.

Sangster, D.F. (1990): Mississippi Valley-type and Sedex lead–zinc deposits: a comparative examination. *Trans. Inst. Min. Metall. (Sect. B, Appl. Earth Sci.)*, **99**, 21–42.

Schneider, J., Haack, U., Hein, U.F., Germann, A. (1999): Direct Rb–Sr dating of sandstone-hosted sphalerites from stratabound Pb–Zn deposits in the northern Eifel, NW Rhenish Massif, Germany. *in* "Mineral deposits: processes to processing", C.J. Stanley *et al*., eds. Balkema, Rotterdam, 1287–1290.

Schwartz, M.O. (2000): Cadmium in zinc deposits: economic geology of a polluting element. *Int. Geol. Rev.*, **42**, 445–469.

Sheffer, H.W. (1966): The occurrence of germanium in willemite. *Geochim. Cosmochim. Acta*, **30**, 837–838.

Simmons, S.F., Kirby, S., Verplanck, P., Kelley, K. (2018): Strategic and critical elements in produced geothermal fluids from Nevada and Utah. *in* "Proceedings 43rd Workshop on Geothermal Reservoir Engineering Stanford University", Stanford, California, February 12–14. SGP-TR-213.

Sintubin, M., Debacker, T.N., Van Baelen, H. (2009): Early Palaeozoic orogenic events north of the Rheic suture (Brabant, Ardenne): a review. *C. R. Geosci.*, **341**, 156–173.

Slezak, P.R., Olivo, G.R., Oliveira, G.D., Dardenne, M.A. (2014): Geology, mineralogy, and geochemistry of the Vazante Northern Extension zinc silicate deposit, Minas Gerais, Brazil. *Ore Geol. Rev.*, **56**, 234–257.

Sweeney, M.A., Patrick, R.A.D., Vaughan, D.J. (1991): The nature and genesis of willemite deposits of Zambia. *in* "Source, transport, and ore deposition of metals", M. Pagel & J. Leroy, eds. Balkema, Rotterdam, 139–142.

Terracciano, R. (2008): Willemite Mineralisation in Namibia and Zambia. PhD Dissertation, Università degli Studi di Napoli Federico II, Napoli, 178 p.

Thiry, M., Quesnel, F., Yans, J., Wyns, R., Vergari, A., Thévenaut, H., Simon-Coinçon, R., Ricordel, C., Moreau, M.-G., Giot, D., Dupuis, C., Bruxelles, L., Barbarand, J., Baele, J.-M. (2006): Continental France and Belgium during the Early Cretaceous: paleoweatherings and paleolandforms. *Bull. Soc. Géol. Fr.*, **177**, 155–175.

Vercautere, C. & van den Haute, P. (1993): Post-Palaeozoic cooling and uplift of the Brabant Massif as revealed by apatite fission track analysis. *Geol. Mag.*, **130**, 639–646.

Verhaert, M., Bernard, A., Dekoninck, A., Lafforgue, L., Saddiqi, O., Yans, J. (2017): Mineralogical and geochemical characterization of supergene Cu-Pb-Zn-V ores in the Oriental High Atlas, Morocco. *Mineral. Deposita,* **52**, 1049–1062.

Wilson, S.A., Ridley, W.I., Koenig, A.E. (2002): Development of sulfide calibration standards for the laser ablation inductively-coupled plasma mass spectrometry technique. *J. Anal. Atom. Spectrom.*, **17**, 406–409.

Yans, J. (2003): An overview of the saprolites of Belgium and their potential kaolinite supplies to Mesozoic and Cainozoic sediments. *Géol. Fr.*, **1**, 33–37.

Ye, L., Cook, N.J., Ciobanu, C.L., Liu, Y.P., Zhang, Q., Liu, T.G., Gao, W., Yang, Y.L., Danyushevskiy, L. (2011): Trace and minor elements in sphalerite from base metal deposits in South China: a LA-ICPMS study. *Ore Geol. Rev.*, **39**, 188–217.

Yesares, L., Saez, R., Nieto, J.M., de Almodovar, G.R., Cooper, S. (2014): Supergene enrichment of precious metals by natural amalgamation in the Las Cruces weathering profile (Iberian Pyrite Belt, SW Spain). *Ore Geol. Rev.*, **58**, 14–26.

Received 7 March 2019
Modified version received 29 May 2019
Accepted 3 June 2019